

Article

# Experimental Evaluation of PM Emission from Red Mud Basins Exposed to Wind Erosion

Valentina Dentoni , Battista Grosso  and Francesco Pinna 

Department of Civil and Environmental Engineering and Architecture (DICAAR), Cagliari University, Via Marengo, 2, 09123 Cagliari, Italy; grosso@unica.it (B.G.); francesco.pinna92@unica.it (F.P.)

\* Correspondence: vdentoni@unica.it

**Abstract:** The disposal of industrial and mineral processing residues represents a major concern for human health and the environment as a whole. In order to reduce the impact on soil and groundwater due to the waste leachability, the implementation of environmental regulations worldwide has favored the conversion of the disposal techniques from wet to dry (i.e., dry stacking or dry disposal). Such a change in the storage practice may cause the increase of particulate matter (PM) emission from the dry surfaces of the tailings exposed to wind erosion. Considering the significance of the environmental issue on a global scale and the increasingly stricter orientation of environmental policies, the need for modeling tools capable of estimating the contribution of tailing basins to air pollution becomes apparent. The paper deals with the disposal of red mud resulting from the bauxite processing in the alumina industry. An experimental research was carried with an environmental wind tunnel to estimate the Emission Factor (EF) of the basin surfaces as a function of the main affecting variables (i.e., residue water content and wind velocity). The article reports the results of the experimental test carried out on the red mud from a major basin located in Sardinia (Italy).



**Citation:** Dentoni, V.; Grosso, B.; Pinna, F. Experimental Evaluation of PM Emission from Red Mud Basins Exposed to Wind Erosion. *Minerals* **2021**, *11*, 405. <https://doi.org/10.3390/min11040405>

Academic Editors:  
George Angelopoulos and Luis Pérez Villarejo

Received: 3 March 2021  
Accepted: 11 April 2021  
Published: 13 April 2021

**Publisher's Note:** MDPI stays neutral with regard to jurisdictional claims in published maps and institutional affiliations.



**Copyright:** © 2021 by the authors. Licensee MDPI, Basel, Switzerland. This article is an open access article distributed under the terms and conditions of the Creative Commons Attribution (CC BY) license (<https://creativecommons.org/licenses/by/4.0/>).

**Keywords:** industrial wind erosion; particulate matter (PM); emission factor (EF); tailings basins; red mud; PM emission factor; environmental impact

## 1. Introduction

The disposal of industrial and mineral processing residues may represent a major environment concern when considering the permanent impact on soil and groundwater due to the leachate filtration through the landfill bottom, as well as the temporary impact on the atmosphere due to the emission of particulate matter (PM) before final capping and revegetation [1,2]. In Europe, the incorporation of the EU Directive [3] into the member states national regulation and the inherent implementation of pertinent BATs (Best Available Techniques) [4] have favored the conversion of the disposal methods from wet (marine discharge and lagooning) to dry (dry stacking and dry disposal). Such a change in the storage practice results in the reduction of the leachability but also in a potential increase of PM emission from the dried surfaces of tailings exposed to wind erosion [5–7]. In fact, due to the significant extent of the disposal areas, as well as to the grain size distribution of the disposed residue, unfavorable meteorological conditions (high temperature, low humidity, intense solar radiation, and wind speed) may cause the emission of large quantities of fine and extra-fine particles (PM<sub>10</sub> and PM<sub>2.5</sub>), which sometimes include inhalable hazardous compounds.

The research hereby discussed specifically deals with the disposal of the residue (red mud) originated from the Bayer process (i.e., production of alumina from bauxite ores). The red mud is composed of fine and very-fine particles and typically presents the mineral composition reported in Table 1 [8]. Table 2 reports the inhalable hazardous substances in the red mud according to international and national indicators: International Agency for Research on Cancer (IARC) [9] classification and Inhalation Unit Risk (IUR) [10,11] for carcinogenic substances and Reference Concentration (RfC) [10,11] for toxic substances.

**Table 1.** Typical mineral composition of the red mud. LOI (loss on ignition) represents the organic and inorganic carbon and water that is chemically bound in the minerals.

Red Mud Components	Typical Content
Fe <sub>2</sub> O <sub>3</sub>	41%
Al <sub>2</sub> O <sub>3</sub>	16%
Na <sub>2</sub> O	4%
SiO <sub>2</sub>	10%
CaO	9%
TiO <sub>2</sub>	9%
LOI	10%
Others	1%

**Table 2.** Inhalable hazardous substances in the red mud according to IARC (International Agency for Research on Cancer), IRIS (Integrated Risk Information System—United States Environmental Protection Agency (USEPA)), and ISS & INAIL (Istituto Superiore di Sanità & Istituto Nazionale per l'Assicurazione contro gli Infortuni sul Lavoro—Italy).

Hazardous Substance	IARC [9]	IRIS [10]	ISS & INAIL [11]
Arsenic—As	1	IUR	IUR, RfC
Beryllium—Be	1	IUR, RfC	IUR, RfC
Cadmium—Cd	1	IUR	IUR, RfC
Nickel—Ni	1	—	IUR, RfC
Lead—Pb	2A	—	IUR, RfC
Mercury—Hg	3	RfC	RfC
Chromium—Cr	2	—	RfC
Hexavalent Chromium—CrVI	1	IUR, RfC	IUR, RfC
Copper—Cu	—	—	RfC
Manganese—Mn	—	RfC	—
Antimony—Sb	—	—	IUR, RfC
Selenium—Se	3	RfC	IUR, RfC
Thallium—Tl	—	—	IUR, RfC
Vanadium—V	—	—	IUR, RfC

IARC (classification of carcinogenic substances); Inhalation Unit Risk (IUR) (estimate of the increased cancer risk from inhalation exposure to a concentration of 1 µg/m<sup>3</sup> for a lifetime); Reference Concentration (RfC) (estimate of a continuous inhalation exposure to human population that is likely to have no appreciable risk of dangerous effects during a lifetime).

A production of mud ranging from 0.7 to 2 tons is actually associated to each ton of alumina, depending on the bauxite characteristics and the processing parameters [12]. In the absence of economically advantageous reuse or recycling alternatives [13,14], the red mud is disposed in Bauxite Residue Disposal Areas (BRDAs). Currently, about 80 alumina plants are active worldwide, with an annual production of residue around 200 million tons (Mt) [15] (Bauxite tailings tonnage was estimated by applying an overall ratio of 1.5 to the alumina production [7,16]). At the present time, the total waste stored in the BRDAs is about 4.5 Bt, which is calculated by summing the production of the last twelve years to the amount stored up to 2008 [16].

Considering the significance of the issue on a global scale and the increasingly stricter orientation of international environmental policies towards a progressive reduction of harmful emissions generated by industrial activities [4,17], the need for reliable modeling tools capable of estimating the contribution of tailing basins to PM air pollution becomes apparent. An experimental research was carried out by means of an environmental wind tunnel, which aims at estimating the Emission Factor (EF) of red mud surfaces exposed to wind erosion as a function of the main affecting variables: mud water content and wind speed. Starting from the conceptual model already proposed in Dentoni et al. [18], which is summarized in paragraph 2, the article discusses the results of the experimental test carried on red mud samples from a major BRDA located in south-eastern Sardinia (Italy).

The experimental plan has been implemented by means of the Environmental Wind Tunnel (EWT) recently designed and built at the Department of Civil and Environmental Engineering and Architecture (DICAAR) of Cagliari University. The experimental procedure and the apparatus set up, thoroughly described in Dentoni et al. [19], were designed on the basis of consistent literature regarding the emission of PM from different types of erodible surfaces [20–25].

### Terminology

Mud particles: elementary particles that form the red mud, individually obtained by suspension of the mud in water.

Plastic mud: mud with water content between the plastic and the liquid limit.

Mud crust: solid state mud (i.e., with water content below the plastic limit) resulting from drying processing.

Crust particles: fragments of crust consisting of dried aggregates of elementary mud particles.

Particles assemblage: set of crust particles and mud particles in a dry state.

## 2. The Conceptual Emission Model

The emission of fine particles from an erodible surface can be initiated either by aerodynamic forces (direct entrainment of particles with diameter less than 70 micron) or by the impact caused by the wind-driven hopping motion (saltation) of sand-sized particles [26–28]. The impact of the saltating particles over the surface produces the expulsion of fine particles (bound to the surface by cohesive forces) and the disintegration of the saltating grains with production of dust (i.e., smaller particles). Many studies have analyzed the influence of the variables affecting the emission phenomenon for a variety of erodible materials [24,29–33]. It is well known that, among other factors, the moisture content plays a fundamental role in triggering the emission [34,35], particularly when the erodible surface is made of fine and very fine particles, as in the case of tailings basins.

The conceptual emission model hereby discussed [18] is based on the observation that the surface of a tailings' deposit assumes relatively homogeneous physical characteristics during rainfall periods, when the humidity of the mud is high (wet season), whereas it is composed of areas with very different physical and emissive characteristics following periods of long exposure to the drying action of the wind and the sun (dry season). According to that, an emission trigger condition has been defined (ON/OFF condition), which is determined by the moisture level of the mud at the surface. In the ON condition, the basin surface can be discretized into three types of emitting surfaces: crust without cracks (S1), crust with cracks (S2), and particles assemblage (S3). Sources of type S1 and S2 are the result of natural drying processes, favored by specific meteorological conditions. Assemblages of free particles (S3) are formed by wind transport and accumulation in morphologically depressed areas. The free particles are aggregates of mud particles and originates from the mechanical disintegration of dried crusts (i.e., wind action on the cracks' thin edges; effect of hails and heavy rains; personnel and vehicles traveling across the basin surface; etc.).

Each type of surface is characterized by its areal distribution over the deposit surface and a specific value of the emission potential. The application of the proposed conceptual model involves the preliminary discretization of the basin surface by means of a square mesh of arbitrary size and the analysis of the mud surface within the mesh cells:

- if a cell contains only one solid continuous element, the surface is assigned to the category S1 (crust without cracks),
- if a cell contains a countable number of continuous solid elements, the surface is assigned to the category S2 (crusts with cracks), and
- if a cell contains an infinite (very large) number of continuous solid elements, the surface is assigned to the category S3 (particle assemblage).

The emission rate ( $E$ ) ( $\text{g s}^{-1}$ ) of the entire surface is then calculated according to Equation (1):

$$E = \sum_{i=1}^3 EF_i \cdot A_i, \quad (1)$$

where  $A_i$  represents the sum of the areas ( $\text{m}^2$ ) of the  $i$ -type surfaces ( $S_i$ ), and  $EF_i$  is the corresponding Emission Factor ( $\text{g}\cdot\text{s}^{-1}\cdot\text{m}^{-2}$ ).

For a given deposit, the discretization of the surface into the sub-emitting areas ( $S_1$ ,  $S_2$  and  $S_3$ ) can be defined by means of appropriate visual tools (i.e., analysis of aerial photographs), while the emission factors  $EF_i$  are expressed by general algorithms as a function of the material physical properties and the wind velocity. Figure 1 shows the discretization of a portion of a red mud surface into emitting sub-areas of type  $S_1$ ,  $S_2$ , and  $S_3$ .

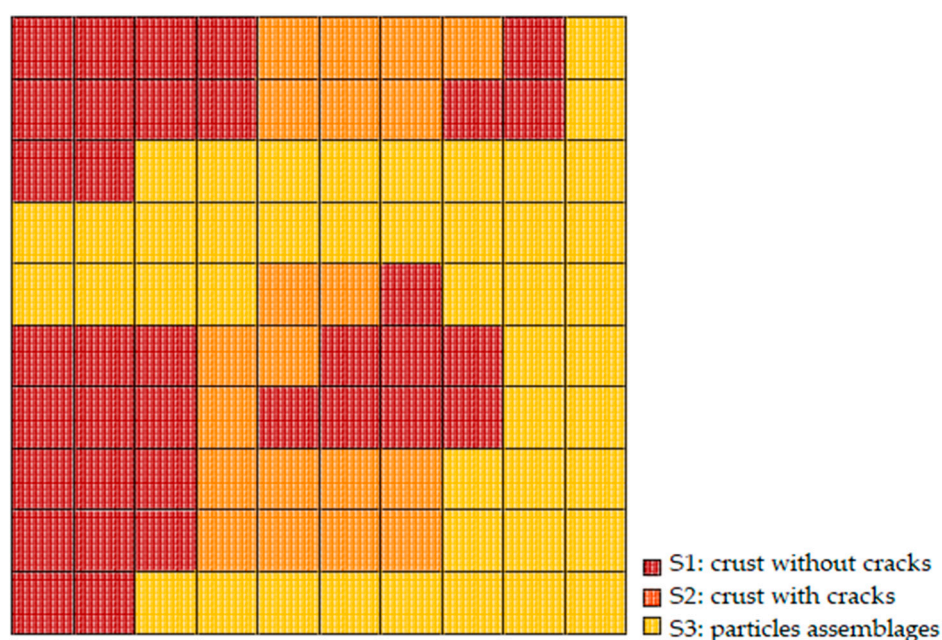


**Figure 1.** Discretization of a portion of the deposit surface into sub-areas  $S_1$ ,  $S_2$ , and  $S_3$ .

The emission factors  $EF_i$  in Equation (1) were experimentally determined on red mud samples subjected to the erosive action of the ABL (Atmospheric Boundary Layer) simulated in the DICAAR EWT [19]. Figure 2 represents the satellite image of the Sardinian BRDA in the Portovesme industrial site (Italy), where the characteristic parameters of the ABL were previously estimated [5,6,8,18,19]. The samples to be tested were prepared in the DICAAR laboratory with the red mud from the Sardinian deposit.

The emission tests were carried out on samples of crusts without cracks ( $S_1$ ) and particles assemblage ( $S_3$ ), while the emission model described by equation (2) was assumed to represent the emission of crusts with cracks ( $S_2$ ). In fact, based on the observation that cracks are grooves totally or partially filled with free particles/particles aggregates, they can be described as two-dimensional elements of particle assemblages of fixed width ( $W$ ) and length per surface unit equal to  $L$ . Assuming the emission factors of  $S_1$  and  $S_3$  are known ( $EF_1$  and  $EF_3$ , respectively), the emission factor of  $S_2$  ( $EF_2$ ) can be calculated according to Equation (2):

$$EF_2 = EF_1 + k L EF_3, \quad (2)$$

where  $k$  is a constant parameter that preliminary can be assumed equal to  $W$ , under the following simplifying assumptions:

- cracks with fixed width ( $W$ ),
- cracks filled up with particles assemblages.



**Figure 2.** Satellite image of the Sardinian Bauxite Residue Disposal Area ( $39^{\circ}10'53''$  N  $8^{\circ}24'30''$  E).

### 3. Materials and Methods

#### 3.1. The DICAAR Environmental Wind Tunnel

The experimental tests aimed at defining the emission factors  $EF_1$  and  $EF_3$  were carried out in the EWT recently designed and built at the DICAAR's laboratories (Cagliari, Italy). The schematic representation of the tunnel is reported in Figure 3, where four main sections of the tunnel are distinguishable: convergent section (CS), flow development section (FDS), test section (TS), and drive section (DS).

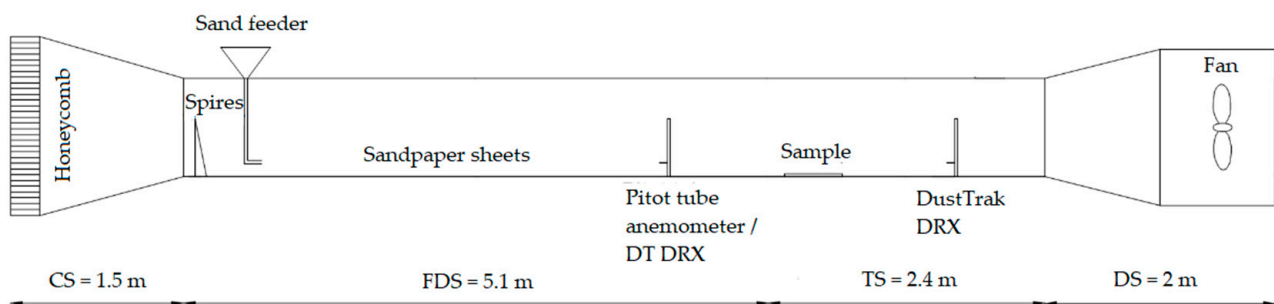


**Figure 3.** Schematic representation of the Department of Civil and Environmental Engineering and Architecture (DICAAR) Environmental Wind Tunnel (EWT).

The FDS section is designed in accordance to the indications of White and Mounla [36], in order to obtain the complete development of the Atmospheric Boundary Layer (ABL) before the TS section. Spires of appropriate size are installed at the entrance of the FDS section to accelerate the growth rate of the ABL [37]. Three-dimensional elements of appropriate size are attached to the FDS floor to simulate the roughness of the erodible surface under investigation. A niche is provided in the pavement of the TS section to insert a tray containing the sample, so that the sample surface and the tunnel floor form a continuous surface of equal roughness. The sample tray is 0.50 m long and 0.20 m wide, as to account for the effect of saltation (i.e., wind-driven hopping motion of coarse

particles/fine particles aggregates which lay on the sample surface) [32]. The test section also houses the air intake lines, which are connected to the measuring instruments outside the tunnel: a Pitot tube anemometer and two dust analysers (DustTrak DRX 8533, TSI, Shoreview, USA). A 5.5 kW axial fan is finally installed in the DS section to provide the required wind flow.

The configuration described above has been recently integrated with a feeding system at the beginning of the FDS to allow the conveyance of sand-sized particles and simulate the effect of saltation in the test section. This recent integration was developed to evaluate the ejection effect of hopping particles, in the absence of free particles on the sample surface.

### 3.2. Wind Tunnel Set Up

For the purposes of the experimental plan hereby discussed, the tunnel was set up to reproduce the characteristic ABL observed above the flat surface of the Sardinian BRDA. The wind speed was measured at two different heights to obtain the mean value of the friction coefficient  $\alpha$  in the Power Law Wind Profile (Equation (3)):

$$u = u_{ref} \left( \frac{z}{z_{ref}} \right)^\alpha, \quad (3)$$

where  $u$  is the wind velocity at the height  $z$ , and  $u_{ref}$  the wind velocity at the reference height  $z_{ref}$ . A characteristic friction coefficient ( $\alpha = 0.10$ ) was calculated with Equation (4):

$$a = \frac{\ln(u_1) - \ln(u_2)}{\ln(z_1) - \ln(z_2)}. \quad (4)$$

In order to simulate the required ABL, two spires of height 53.0 cm ( $h_s$ ) and base 3.5 cm ( $b_s$ ) were installed at the tunnel entrance. The two-dimensional parameters were calculated by means of the following Equations (5) and (6) [37]:

$$h_s = \left( \frac{1.39 \delta}{1 + \frac{\alpha}{2}} \right)^\alpha, \quad (5)$$

$$\frac{b_s}{h_s} = 0.5 \left[ \frac{\psi \left( \frac{H}{\delta} \right)}{1 + \psi} \right] \left( 1 + \frac{\alpha}{2} \right), \quad (6)$$

where  $\alpha$  is the required friction coefficient (0.10 in this case), and  $\delta$  is the ABL thickness inside the tunnel (corresponding to  $z_{ref}$  in Equation (3)),  $u_\delta$  is the wind velocity at  $\delta$  (corresponding to  $u_{ref}$  in Equation (3)), and  $\psi$  is a function of  $\alpha$  e  $\delta$  [37]. The ABL thickness  $\delta$  was set at 40.0 cm from the tunnel floor, about half the tunnel height [38].

The tunnel floor was coated with an 80-grit sandpaper (corresponding to particles size around 200 micron) to simulate the roughness of the red mud surface along the FDS.

Wind speed tests were performed at the test section to verify the consistency of the simulated wind profiles: the results proved the tunnel to be capable of simulating the required ABL for operating condition of the fan between 15 and 45 Hz, which correspond to mean velocity at 40 cm ( $z = \delta$ ) in the range 5.47–18.29 m·s<sup>-1</sup>.

### 3.3. Preparation of Samples

The experimentation was carried out on representative samples of the two types of surface S1 and S3 (laboratory samples), which were prepared in the DICAAR laboratories starting from the mud in its plastic state collected on site (at the Sardinian BRDA). The main properties of the red mud in its plastic state were primarily estimated (particle-size distribution, specific weight of grains, water content, and porosity). Actual samples of crusts and particle assemblages (field samples) were also collected at the BRDA, in

order to identify the physical characteristics of the emitting surfaces to be reproduced in the laboratory.

### 3.3.1. Samples of Particles Assemblages

The field samples of particle assemblages were characterized according to their particle-size distribution (PSD) and physical properties. Table 3 represents the mean PSD of the field samples obtained by dry sieve analysis [39], which allows the characterization of the particles assemblage without disintegrating the aggregates formed by elementary particles bound together by surface forces (inter-particles forces). Table 4 reports the mean values of the physical parameters assumed as target values to process the 5 laboratory samples to be tested in the environmental wind tunnel.

**Table 3.** Mean particle size distribution of field samples (S3—particles assemblage).

Diameter (mm)	<0.125	0.125–0.250	0.250–0.500	0.500–1	>1
Mean frequency (%)	37	22	20	18	3

**Table 4.** Mean values of the field samples physical parameters (S3—particles assemblages).

	Apparent Dry Density ISO 11272:2017 [40] (kg·m <sup>-3</sup> )	Moisture Content <sup>1</sup> (%)	Void Ratio <sup>1</sup>
Mean value	1200	3	1.6
Standard deviation	50	1.3	0.5

<sup>1</sup> The void index and moisture content were calculated with reference to a value of particles density equivalent to that of the crusts, assuming that the particles assemblages are formed by aggregates of particles deriving from the disintegration of crusts.

The laboratory samples were prepared according to the following procedure:

1. Oven-drying of the mud at 40 °C, for the time necessary to obtain a crust with the density value close to that of the field samples.
2. Manual disintegration of the crust (with pestle and mortar) and subsequent granulometric analysis of the granular material, until a particle-size distribution equivalent to that of the field samples is obtained.
3. Material arrangement in the sample tray and thickening up to dry density equivalent to that of the field samples.
4. Wetting up to the required experimental moisture content, as defined in the experimental plan. Each sample was then left in a sealed container for a period of 12 h to favor the homogenization of the water content.

### 3.3.2. Samples of Crusts

The mean physical parameters of the crusts collected at the BRDA are reported in Table 5. The laboratory samples were built by subjecting the dried and disintegrated material obtained through the steps 1 to 3 of the procedure above described to the following additional processing steps:

1. Surface wetting up to water content of about 30% (corresponding to that of the mud in its plastic state).
2. Exposure to solar radiation and wind (natural drying process) to obtain crusts with specific weight and moisture content comparable to those of the field samples.

Previous studies have discussed the effect of carbonation/decarbonation in the formation of surface aggregates [41–43]. The specific role of atmospheric carbon dioxide on the formation of crusts is not discussed in this article. However, the crust samples were built under natural environmental condition, thus the results of the experimental test hereby reported are implicitly affected by carbonation.

**Table 5.** Mean values of the field samples physical parameters (S1—crust without cracks).

	Apparent Dry Density ISO 17892-2:2014 [44] ( $\text{kg}\cdot\text{m}^{-3}$ )	Moisture Content (%)	Void Ratio
Mean value	1700	3	0.8
Standard deviation	73	1.5	0.2

Figure 4 shows the images of the 2 type of laboratory samples (S1 and S3).

**Figure 4.** Trays (0.50 m long  $\times$  0.20 m wide) containing the two types of laboratory samples: granular material after disintegration (a) and crusts without cracks (b).

### 3.4. The Experimental Plan

The wind tunnel tests were carried out both for particles assemblages and crusts with wind friction velocities ( $u_*$ ) in the range 0.23 to 0.54  $\text{m}\cdot\text{s}^{-1}$ . The experimental  $u_*$  values were obtained by fitting the log-law profile equation (i.e., Law of the Wall) with the wind speed values measured in the tunnel, downstream of the test section: they correspond to wind velocity at 40 cm ( $\delta$ ) in the range between 5.44  $\text{m}\cdot\text{s}^{-1}$  and 16.19  $\text{m}\cdot\text{s}^{-1}$ .

A moisture content ( $w$ ) from 0 to 24% was investigated for particles assemblages, after the preliminary validation of the OFF condition (i.e., zero emission) for samples with 30% water content. For each combination  $u_*$ - $w$ , the wind speed and the PM concentration were measured downstream of the test section in 9 points between 2.5 and 40 cm ( $\delta$ ) along the tunnel vertical axis of symmetry. The set of measurements was repeated for each of the 5 samples of particles aggregates (1350 measurements).

The tests on the mud crusts (with  $w = 3\%$ ) were carried out both with and without the conveyance of additional saltators ( $F = 7 \text{ g}\cdot\text{s}^{-1}$  of sand-sized particles with  $d = 200 \mu\text{m}$ ), in order to investigate the effect of saltation in the lack of free bouncing particles/aggregates on the crust surface. Each set of measurements (the 9 measurement points above mentioned) was repeated for the 3 samples of crusts (324 measurements).

### 3.5. Estimate of PM10 Emission

The PM10 emission rate ( $E$ ) has been estimated in accordance to the control volume method proposed by Roney and White [20], where the control volume is the product of the

surface of a given erodible surface  $A$  by the height of the boundary layer generated in the tunnel ( $\delta$ ). The emission rate  $E$  is expressed by Equation (7):

$$E = \frac{1}{A}(m_{out} - m_{in}), \quad (7)$$

where  $m_{out}$  and  $m_{in}$  are, respectively, the mass flow of particle matter exiting and entering the control volume and are calculated through Equations (8) and (9):

$$m_{out} = \int_0^\delta c_{out} u_{out} W dz, \quad (8)$$

$$m_{in} = \int_0^\delta c_{in} u_{in} W dz, \quad (9)$$

where  $c_{out}$  and  $c_{in}$  are the PM concentration values measured downstream and upstream of the test section, respectively (from 0 to  $\delta$ );  $u_{out}$  and  $u_{in}$  are the corresponding velocity values (i.e., measured at the corresponding points);  $W$  (0.20 m) is the sample's width;  $\delta$  (0.40 m) is the depth the simulated ABL (maximum height of the ABL reproduced in the tunnel test section). The concentration  $c_{in}$  was assumed to be equal to the background concentration monitored before each test, which was always less than  $0.03 \text{ mg}\cdot\text{m}^{-3}$ . The velocity profiles upstream and downstream of the test section were assumed to be coincident. The emission rate  $E$ , expressed as mass of particulate matter (PM) emitted by the surface unit in the unit time ( $\text{g}\cdot\text{m}^{-2}\cdot\text{s}^{-1}$ ), is given by Equation (10), where  $L$  (0.50 m) is the sample's length.

$$E = \frac{1}{L} \int_0^{H_\delta} (c_{out} u_{out} - c_{in} u_{in}) dz. \quad (10)$$

Figure 5 shows the longitudinal cross section of the DICAAR EWT, with the indication of measurement instruments before and after the sample tray.

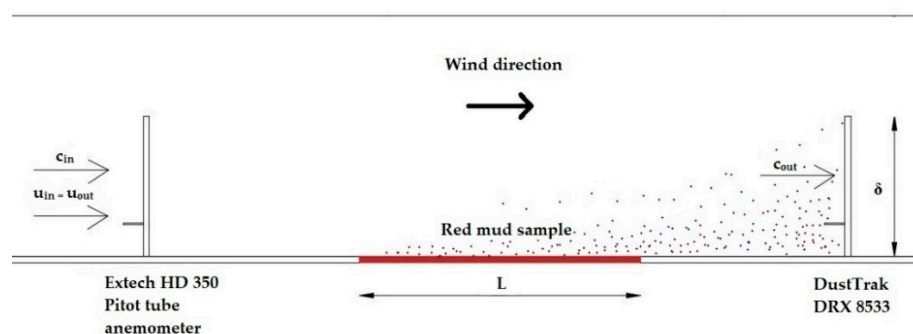


**Figure 5.** Schematic representation of the test section in the EWT: location of measurement instruments (pitot tube and dust analyzer) and tray with red mud sample (control volume method).

## 4. Results

### 4.1. Emission Rates of Particles Assemblages

Based on the measurement results, the mean profiles of PM<sub>10</sub> concentration ( $C_{PM10}$ ) were elaborated for each  $u_*-w$  pair in the experimental plan. Figure 6 shows the mean concentration profiles for the investigate values of  $u_*$  and  $w = 0\%$ , with the exception of  $u_* = 0.23 \text{ m/s}$ , as the concentration value were  $\approx 0$  along the entire tunnel height. Each  $C_{PM10}$  value diagrammed in Figure 6 (with different color, depending on the experimental shear velocity) is the arithmetic mean of the time-averaged concentration values measured in the same point.

The unitary emission rates ( $E_{PM10}$ ) reported in Table 6 were calculated for each  $u_*-w$  combination by means of Equation (10): the data confirms the  $E_{PM10}$  growth with increasing friction velocity and decreasing water content.

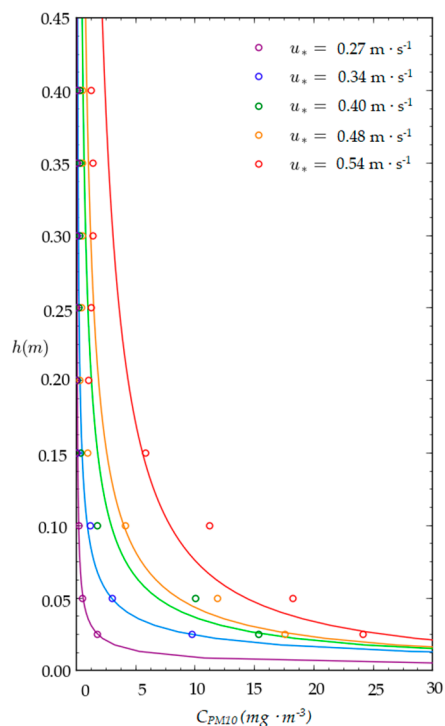


**Figure 6.** Experimental profiles of particulate matter (PM10) mean concentration ( $C_{PM10}$ ) for dry samples (S3).

**Table 6.** Calculated values of emission rates ( $E_{PM10}$ ) for each  $u_*-w$  combination in the experimental plan (S3).

$u_*$ $m \cdot s^{-1}$	$u_\delta$ $m \cdot s^{-1}$	$u_{10}$ $m \cdot s^{-1}$	$E_{PM10} (mg \cdot m^{-2} \cdot s^{-1})$				
			0%	2%	8%	16%	24%
0.23	5.47	7.13	0.08	0.02	0.01	0.00	0.00
0.27	7.63	9.48	1.10	0.58	0.06	0.08	0.05
0.34	9.82	12.20	8.26	2.89	1.25	1.05	0.33
0.40	11.93	14.83	21.17	10.14	5.90	3.62	0.49
0.48	14.11	17.66	32.47	29.93	19.76	9.66	5.83
0.54	16.19	20.08	72.63	65.22	30.95	28.72	10.70

#### 4.1.1. Emission Rates vs. Wind Velocity

According to the scientific literature, the emission rate can be described by the general power law  $E = a \cdot u_*^b$  [30]. With reference to the investigated values of surface moisture content, Table 7 and Figure 7 summarize the results of the power law fitting to the experimental data: a very good correlation ( $R^2$  between 0.98 and 0.99) was found between the emission rate ( $E_{PM10}$ ) and the shear velocity ( $u_*$ ) for all the experimental values of moisture content.

**Table 7.** Results of the power law fitting to the experimental data (S3)— $E = a \cdot u_*^b$ .

$w$	$a$	$b$	$R^2$
0%	1595	5.1	0.98
2%	3516	6.5	0.99
8%	732	5.1	0.98
16%	5290	8.5	0.99
24%	659	6.6	0.98

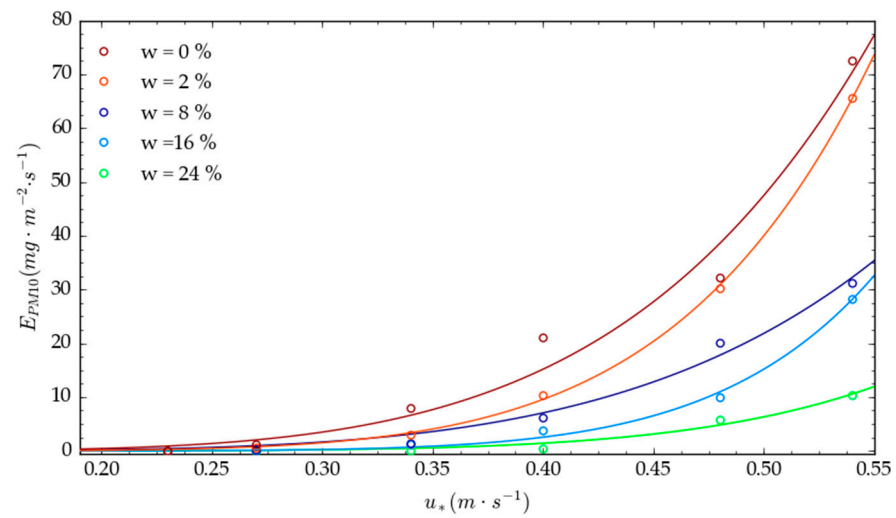


Figure 7. Results of the power law fitting to the experimental data.

#### 4.1.2. Emission Rates vs. Surface Water Content

The correlation between the unitary emission rate ( $E_{PM10}$ ) and the water content ( $w$ ) was also analyzed for all the experimental friction velocities except for the lowest value ( $0.23 \text{ m}\cdot\text{s}^{-1}$ ), as in that case the emission was found negligible. A very good negative correlation was found ( $R^2$  between 0.91 and 0.99) by fitting the general equation  $E = a \cdot b^w$  to the experimental data. The results are reported in Table 8 and graphically represented in Figure 8.

Table 8. Results of the power law fitting to the experimental data (S3)— $E = a \cdot b^w$ .

$u_*$ ( $\text{m}\cdot\text{s}^{-1}$ )	$a$	$b$	$R^2$
0.27	1.1	0.72	0.99
0.34	8.2	0.62	0.94
0.40	19.2	0.84	0.91
0.48	33.4	0.93	0.99
0.54	72.6	0.93	0.95

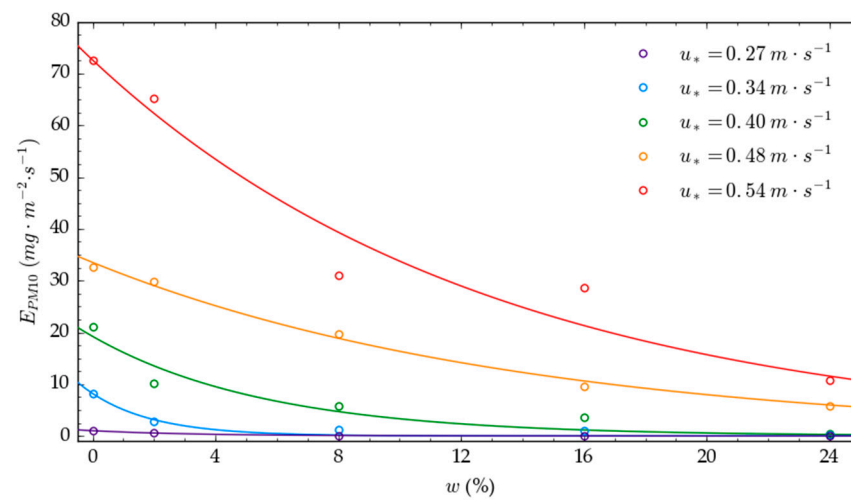


Figure 8. Results of the exponential law fitting to the experimental data (S3).

#### 4.1.3. Emission Rates vs. Surface Water Content and Shear Velocity

A bivariate analysis was performed to express the dependence of the unitary emission rate on the water content and friction velocity in a single equation  $EF = f(u_*, w)$ . A

commercial curve fitting and data analysis software (*CurveExpert Professional*) was used to analyze the experimental data. Equation (11) consistently describes ( $R^2 = 0.98$ ) the emission factor of the particles assemblages.

$$EF = a u_*^b c^w \tag{11}$$

The values of the parameters  $a$ ,  $b$ , and  $c$  in Equation (11) depend on the physical characteristics of the material (grain-size, surface roughness, particle density, and inter-particle forces). In the case study hereby discussed, they assume the following values:  $a = 2417$ ,  $b = 5.7$ , and  $c = 0.93$ . The emission factor ( $EF$ ) is graphically represented in Figure 9.

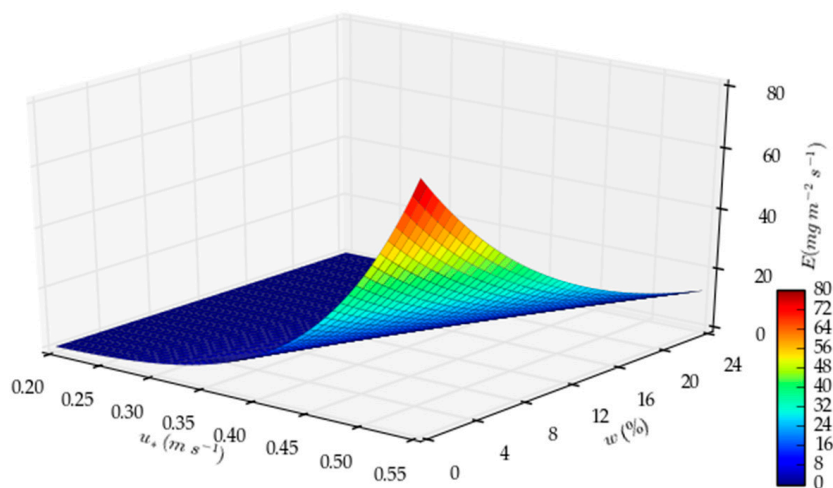


Figure 9. Graphical representation of Emission Factor (S3).

#### 4.2. Emission Rates of Crusts

Insignificant values of PM10 concentration were measured for crusts in the absence of the additional saltators; hence, no dust profiles are provided in this case.

Table 9 reports the values of the unitary emission rate ( $E_{PM10}$ ) of crusts subjected to the additional flow of saltating particles (S1). Its dependence on the friction velocity ( $u_*$ ) is consistently described by the equation  $EF = a \cdot u_*^b$  ( $R^2 = 0.94$ ,  $a = 516$ ,  $b = 5.9$ ), which represents the emission factor for crusts without cracks, as defined in the conceptual emission model. Figure 10 reports the graphical representation of the Emission rate ( $E_{PM10}$ ) of crust samples with additional saltators (S1).

Table 9. Calculated values of emission rates from crust samples with additional saltators (S1).

$u_*$ $m \cdot s^{-1}$	$u_\delta$ $m \cdot s^{-1}$	$u_{10}$ $m \cdot s^{-1}$	$E_{PM10}$ $mg \cdot m^{-2} \cdot s^{-1}$
0.23	5.47	7.13	0.00
0.27	7.63	9.48	0.55
0.34	9.82	12.20	2.69
0.40	11.93	14.83	3.10
0.48	14.11	17.66	4.85
0.54	16.19	20.08	13.86

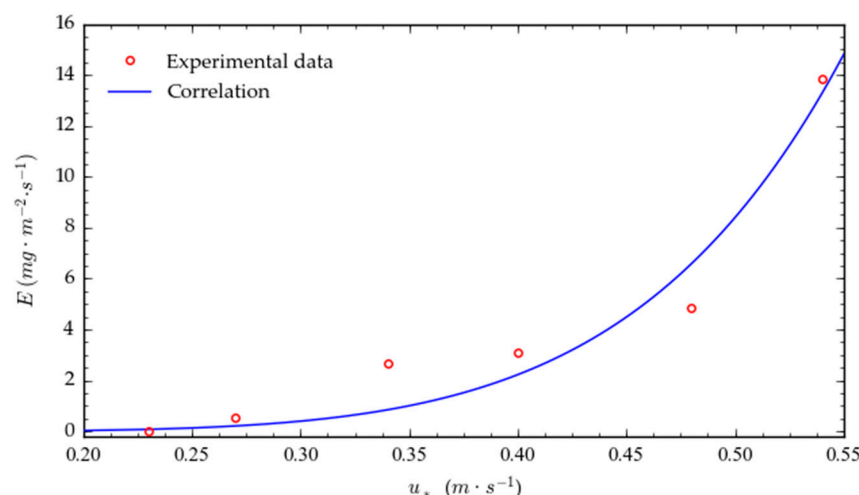


Figure 10. Emission rate ( $E_{PM10}$ ) of crust samples with additional saltators (S1).

## 5. Discussion

The main result of the study hereby discussed is the definition of the algorithms that describe the emission potential of a BRDA (Equation (1)). The Emission Factors (EFs) resulting from the experimental tests appear reliable, considering the number of measurements performed for each condition and the low statistical dispersion of the results.

In particular, the tests performed on mud crusts proved that, despite their very low water content, crusted surfaces only emit if subjected to the impact of saltating particles [32,45]. Under natural conditions, the saltating particles are represented by free particles aggregates, which mainly derive from crusts disintegration. In such a condition, the emission potential is described by the exponential function  $EF = a \cdot u_*^b$ , where  $a$  and  $b$  are the site-specific parameters. The experimentation can be eventually finalized by verifying the validity of the prediction model proposed for crusts with cracks (i.e., Equation (2)), aimed at defining the value of the parameter  $K$ , which in this phase is assumed equal to the average cracks width ( $W$ ).

The results of the tests performed on particles assemblages were found in accordance with previous experimental studies [21,24,30,31,46]. It was found that the equation  $EF = a u_*^b c^w$  consistently describes the emission from particles assemblages, where the parameters  $a$ ,  $b$ , and  $c$  are specific for the bauxite residue. The same experimental procedure can be applied to different tailings to estimate the corresponding site-specific parameters ( $a$ ,  $b$ , and  $c$ ).

It should be noted that the application of the proposed methodology also requires the preliminary characterization of the approaching wind profile (ABL) and its correct simulation by means of an Environmental Wind Tunnel (EWT).

In conclusion, the following practical implications derive from this research study:

- the definition of a general methodology to be applied to fugitive dust sources (open storage, mine dumps and waste deposits);
- the availability of a specific conceptual emission model for tailings (very fine erodible material with unlimited emission potential) (Equation (1));
- the availability of specific algorithms (EFs) to be used as input parameters in the prediction of PM air dispersion (i.e., implementation of dispersion modeling codes), typically required within the Environmental Impact Assessment procedures (EIA) [3];
- the availability of a practical operative tool for the estimation of the moisture cut-off grade, which guarantees the respect of the concentration limit values established by law [3] at a given receptor and for a given wind velocity.

With reference to the last point above mentioned, the attached reference document (Table S1) reports the calculation of the moisture cut-off grades ( $w$ ) as a function of the wind velocity ( $u_{10}$ ) measured at 10 m above the basin surface, under the assumption of

uniform emitting surface of particles assemblages (S3) and predicted value of threshold emission rate  $E = 2 \text{ (mg}\cdot\text{m}^{-2}\cdot\text{s}^{-1})$ . The threshold emission rate ( $E$ ) corresponds to a PM10 concentration at a given hypothetical receptor equal to the *limit value* established by law [3] and depends on the specific case under investigation (source's areal extent, source-receptor distance, orography of the impact territory, meteorological conditions, etc.). The threshold emission rate ( $E$ ) can be calculated by performing a back analysis with an appropriate dispersion modeling code [47].

## 6. Conclusions

An experimental research was carried out to estimate the emission potential of a red mud basin (i.e., Bauxite Residue Disposal Area) exposed to wind erosion (i.e., industrial wind erosion). PM10 emission tests were performed by means of an environmental wind tunnel to define the Emission Factors (EFi) of three types of emitting surfaces: crust without cracks (S1), crust with cracks (S2), and particles assemblage (S3).

The three Emission Factors are integrated into a single equation that describes the overall emission of a tailings basin surface as a function of the wind velocity and the mud moisture content. The experimental results were found statistically reliable and consistent with the scientific literature.

The proposed emission model has general validity and may represent a valuable contribution to the environmental impact assessment (EIA) studies regarding the management of tailings basins, which commonly require the implementation of dispersion modeling codes to predict the PM air dispersion within the impact territory on the base of consistent site-specific emission factors.

**Supplementary Materials:** The following are available online at <https://www.mdpi.com/article/10.3390/min11040405/s1>, Table S1: Calculation of the moisture cut-off grades when the predicted threshold value of PM10 emission rate is  $E = 2 \text{ mg}\cdot\text{m}^{-2}\cdot\text{s}^{-1}$ .

**Author Contributions:** Conceptualization, methodology & supervision, B.G. and V.D.; investigation and data curation, F.P.; writing & original draft preparation, V.D. and F.P.; writing & final review, B.G. and V.D. All authors have read and agreed to the published version of the manuscript.

**Funding:** The research was funded by the Fondazione di Sardegna and Regional Sardinian Government (Grant CUP F72F16003160002).

**Acknowledgments:** Investigation carried out in the framework of projects conducted by CINIGeo (National Inter-university Consortium for Georesources Engineering Rome, Italy) and CESA (Center of excellence of environmental sustainability).

**Conflicts of Interest:** The authors declare no conflict of interest.

## References

1. Higgins, D.; Curtin, T.; Courtney, R. Effectiveness of a constructed wetland for treating alkaline bauxite residue leachate: A 1-year field study. *Environ. Sci. Pollut. Res.* **2017**, *24*, 8516–8524. [CrossRef] [PubMed]
2. Ren, J.; Chen, J.; Han, L.; Wang, M.; Yang, B.; Du, P.; Li, F. Spatial distribution of heavy metals, salinity and alkalinity in soils around bauxite residue disposal area. *Sci. Total Environ.* **2018**, *628–629*, 1200–1208. [CrossRef] [PubMed]
3. European Union (EU). Directive 2008/50/EC of the European Parliament and of the Council of 21 May 2008 on Ambient Air Quality and Cleaner Air for Europe. 2008. Available online: <https://eur-lex.europa.eu/legal-content/en/ALL/?uri=CELEX%3A32008L0050> (accessed on 3 August 2020).
4. European Commission (EC). Reference Document on Best Available Techniques on Emissions from Storage. 2006. Available online: <https://eippcb.jrc.ec.europa.eu/reference/> (accessed on 1 September 2020).
5. Cigagna, M.; Dentoni, V.; Grosso, B.; Massacci, G. Fugitive Dust Emissions Due to the Disposal of Dried Red Mud. In Proceedings of the 14th International Waste Management and Landfill Symposium, Pula, Italy, 30 September–4 October 2013.
6. Dentoni, V.; Grosso, B.; Levanti, C.; Massacci, G. PM emissions from a BR basin and impact assessment on air quality. In Proceedings of the 23rd International Symposium on Mine Planning and Equipment Selection, Johannesburg, South Africa, 9–11 November 2015.
7. Power, G.; Gräfe, M.; Klauber, C. Bauxite residue issues: I. Current management, disposal and storage practices. *Hydrometallurgy* **2011**, *108*, 33–45. [CrossRef]

8. Dentoni, V.; Grosso, B.; Massacci, G. Environmental sustainability of the alumina industry in Western Europe. *Sustainability* **2014**, *6*, 9477–9493. [CrossRef]
9. International Agency for Research on Cancer. IARC Monographs on the Identification of Carcinogenic Hazards to Humans. Available online: <https://monographs.iarc.who.int/list-of-classifications/> (accessed on 29 March 2021).
10. United States Environmental Protection Agency (USEPA). IRIS Assements. Available online: [https://iris.epa.gov/AtoZ/?list\\_type=alpha](https://iris.epa.gov/AtoZ/?list_type=alpha) (accessed on 1 April 2021).
11. ISS-INAIL Banca Dati ISS-INAIL per L'analisi Di Rischio Sanitario E Ambientale. Available online: <https://www.minambiente.it/bonifiche/gruppi-e-tavoli-di-lavoro-> (accessed on 1 April 2021).
12. International Aluminium Institute (IAI) and European Aluminium (EA). Bauxite Residue Management: Best Practice. 2015. Available online: <https://bauxite.world-aluminium.org/refining/bauxite-residue-management.html> (accessed on 26 July 2020).
13. Mombelli, D.; Barella, S.; Gruttadauria, A.; Mapelli, C. Iron Recovery from Bauxite Tailings Red Mud by Thermal Reduction with Blast Furnace Sludge. *Appl. Sci.* **2019**, *9*, 4902. [CrossRef]
14. Evans, K. The History, Challenges, and New Developments in the Management and Use of Bauxite Residue. *J. Sustain. Metall.* **2016**, *2*. [CrossRef]
15. International Aluminium Institute (IAI). Alumina Production. Available online: <https://www.world-aluminium.org/statistics/alumina-production/#data> (accessed on 1 February 2021).
16. Klauber, C.; Grafe, M.; Power, G. *Review of Bauxite Residue "Re-Use" Options*; CSIRO: Floreat, Australia, 2009.
17. European Commission. *Best Available Techniques (BAT) Reference Document for the Non-Ferrous Metals Industries—Industrial Emissions Directive 2010/75/EU (Integrated Pollution Prevention and Control.)*; Publications Office of the European Union: Mercier, Luxembourg, 2017. [CrossRef]
18. Dentoni, V.; Grosso, B.; Massacci, G.; Cigagna, M.; Levanti, C.; Corda, C.; Pinna, F. Industrial Wind Erosion: PM Emission from the Erodible Flat Surfaces of Tailing Basins. In Proceedings of the 18th Symposium on Environmental Issues and Waste Management in Energy and Mineral Production; Springer International Publishing: Berlin/Heidelberg, Germany, 2019; pp. 15–27. [CrossRef]
19. Dentoni, V.; Grosso, B.; Massacci, G.; Pinna, F. Validation of a wind erosion model for tailings basins: Wind tunnel design and atmospheric boundary layer simulation. *Int. J. Min. Reclam. Environ.* **2020**. [CrossRef]
20. Roney, J.A.; White, B.R. Estimating fugitive dust emission rates using an environmental boundary layer wind tunnel. *Atmos. Environ.* **2006**, *40*, 7668–7685. [CrossRef]
21. McKenna, C.; Boulton, J.W.; Sanderson, S. Wind tunnel simulation of environmental controls on fugitive dust emissions from mine tailings. *Atmos. Environ.* **2009**, *43*, 520–529. [CrossRef]
22. AVECILLA, F.; Panebianco, J.E.; Buschiazzo, D.E. A wind-tunnel study on saltation and PM 10 emission from agricultural soils. *Aeolian Res.* **2016**, *22*, 73–83. [CrossRef]
23. Panebianco, J.E.; Mendez, M.J.; Buschiazzo, D.E. PM10 Emission, Sandblasting Efficiency and Vertical Entrainment During Successive Wind-Erosion Events. *Bound. Layer Meteorol.* **2016**, *161*, 335–353. [CrossRef]
24. Wei, W.U.; Ping, Y.A.N.; Yong, W.; Miao, D.; Xiaonan, M.; Xinran, J.I. Wind tunnel experiments on dust emissions from different landform types. *J. Arid Land* **2018**, *10*, 548–560. [CrossRef]
25. Sanderson, R.S.; McKenna Neuman, C.; Boulton, J.W. Windblown fugitive dust emissions from smelter slag. *Aeolian Res.* **2014**, *13*, 19–29. [CrossRef]
26. Bagnold, R.A. *The Physics of Blown Sand and Desert Dunes*; Methuen: New York, NY, USA, 1941; ISBN 9789400956827.
27. Shao, Y.; Raupach, M.R.; Findlater, P.A. Effect of saltation bombardment on the entrainment of dust by wind. *J. Geophys. Res.* **1993**, *98*, 12719–12726. [CrossRef]
28. Gillette, D.A. Production of dust that may be carried great distances. *Spec. Pap. Geol. Soc. Am.* **1981**, *186*, 11–26. [CrossRef]
29. Kok, J.F.; Parteli, E.J.R.; Michaels, T.I.; Karam, D.B.; Pierre, U. The physics of wind-blown sand and dust. *Rep. Prog. Phys.* **2012**, *75*, 1–119. [CrossRef] [PubMed]
30. Shao, Y. *Physics and Modelling of Wind Erosion (Atmospheric and Oceanographic Sciences Library, 37)*; Springer: Berlin/Heidelberg, Germany, 2008; ISBN 978-1-4020-8894-0.
31. Nickling, W.G.; Gillies, J.A. Dust emission and transport in Mali, West Africa. *Sedimentology* **1993**, *40*, 859–868. [CrossRef]
32. Gillette, D. A wind tunnel simulation of the erosion of soil: Effect of soil texture, sandblasting, wind speed, and soil consolidation on dust production. *Atmos. Environ.* **1978**, *12*, 1735–1743. [CrossRef]
33. Gillette, D.A.; Blifford, I.H.; Fryrear, D.W. The influence of wind velocity on the size distributions of aerosols generated by the wind erosion of soils. *J. Geophys. Res.* **1974**, *79*, 4068–4075. [CrossRef]
34. Funk, R.; Reuter, H.I.; Hoffmann, C.; Engel, W.; Öttl, D. Effect of moisture on fine dust emission from tillage operations on agricultural soils. *Earth Surf. Process. Landf.* **2008**, *33*, 1851–1863. [CrossRef]
35. Fécan, F.; Marticorena, B.; Bergametti, G. Parametrization of the increase of the aeolian erosion threshold wind friction velocity due to soil moisture for arid and semi-arid areas. *Ann. Geophys.* **1998**, *17*, 149–157. [CrossRef]
36. White, B.R.; Mounla, H. An experimental study of Froude number effect on wind-tunnel saltation. In *Aeolian Grain Transport 1*; Springer: Vienna, Austria, 1991; pp. 145–157.
37. Irwin, H.P.A.H. The design of spires for wind simulation. *J. Wind Eng. Ind. Aerodyn.* **1981**, *7*, 361–366. [CrossRef]
38. Al-Nehari, H.A.; Abdel-Rahman, A.K.; El-Moneim Nassib, A.; Shafey, H.M. Design and Construction of a Wind Tunnel for Environmental Flow Studies. *JES J. Eng. Sci.* **2010**, *38*, 177–193.

39. ASTM C136/C136M—19 Standard Test Method for Sieve Analysis of Fine and Coarse Aggregates. Available online: <https://www.astm.org/Standards/C136> (accessed on 23 February 2021).
40. ISO 1172:2017 Soil Quality—Determination of Dry Bulk Density. Available online: <https://www.iso.org/standard/68255.html> (accessed on 12 February 2021).
41. Klauber, C.; Harwood, N.; Hockridge, R.; Middleton, C. Proposed mechanism for the formation of dust horizons on bauxite residue disposal areas. In Proceedings of the TMS Light Metals, New Orleans, LA, USA, 9–13 March 2008; pp. 19–24.
42. Xue, S.; Ye, Y.; Zhu, F.; Wang, Q.; Jiang, J.; Hartley, W. Changes in distribution and microstructure of bauxite residue aggregates following amendments addition. *J. Environ. Sci. (China)* **2019**, *78*, 276–286. [[CrossRef](#)] [[PubMed](#)]
43. Rai, S.; Wasewar, K.L.; Agnihotri, A. Treatment of alumina refinery waste (red mud) through neutralization techniques: A review. *Waste Manag. Res.* **2017**, *35*, 563–580. [[CrossRef](#)]
44. ISO 17892-2:2014 Geotechnical Investigation and Testing—Laboratory Testing of Soil—Part 2: Determination of Bulk Density. Available online: <https://www.iso.org/standard/55244.html> (accessed on 12 February 2021).
45. Gomes, L.; Arrúe, J.L.; López, M.V.; Sterk, G.; Richard, D.; Gracia, R.; Sabre, M.; Gaudichet, A.; Frangi, J.P. Wind erosion in a semiarid agricultural area of Spain: The WELSONS project. In *Catena*; Elsevier: Amsterdam, The Netherlands, 2003; Volume 52, pp. 235–256. [[CrossRef](#)]
46. Gillette, D.A. Fine Particulate Emissions due to Wind Erosion. *Trans. Am. Soc. Agric. Eng.* **1977**, *20*, 890–897. [[CrossRef](#)]
47. United States Environmental Protection Agency (USEPA). Air Quality Dispersion Modeling | Support Center for Regulatory Atmospheric Modeling (SCRAM) | US EPA. Available online: <https://www.epa.gov/scram/air-quality-dispersion-modeling> (accessed on 1 April 2021).